Chapter 2

Theory and methods

The two key areas of this project cover two widely different fields; crystallisation theory, which is covered in the previous introduction section, and tweezing theory. The following chapter summarises the working principles behind optical tweezing, the differences in scattering theories, and the broader theoretical calculations used throughout the rest of the Thesis.

2.1 Electromagnetism and optical tweezing

Proper understanding of optical tweezing requires an understanding of how the trapped particle interacts with the trapping laser. From an electromagnetism perspective the laser creates a spatially and temporally coherent electric field that scatters light off of a trapped particle. The laws governing electric and magnetic fields are summarised most succinctly via the Maxwell equations. The differential forms of which are given below [1]:

$$\nabla \cdot \mathbf{E} = \frac{\rho_v}{\epsilon_0} \tag{2.1}$$

$$\nabla \cdot \mathbf{B} = 0 \tag{2.2}$$

$$\nabla \times \mathbf{E} = \frac{\partial \mathbf{B}}{\partial t} \tag{2.3}$$

$$\nabla \times \mathbf{B} = \mathbf{j} + \frac{\partial \mathbf{E}}{\partial t} \tag{2.4}$$

where ρ_v is the free charge density, $\mathbf{j}_0$ is the charge current, and ϵ_0 is the permittivity of free space.

These four equations describe how the electric and magnetic fields behave and relate to one another at a microscopic level. Any discussion of optical trapping is underpinned by the fact that in all cases the Maxwell equations must be satisfied at the macroscopic level, where one must account for the medium's interactions with the EM field. Macroscopic forms of the Maxwell equations are given below [1]:

$$\nabla \cdot \mathbf{D} = \rho_f \tag{2.5}$$

$$\nabla \cdot \mathbf{B} = 0 \tag{2.6}$$

$$\nabla \times \mathbf{E} = \frac{\partial \mathbf{B}}{\partial t} \tag{2.7}$$

$$\nabla \times \mathbf{H} = \mathbf{J}_f + \frac{\partial \mathbf{D}}{\partial t} \tag{2.8}$$

Where ρ_f and $\mathbf{J}_f$ are the charge density and current caused by the presence of free charges in the medium, and $\mathbf{D}$ and $\mathbf{H}$ are the displacement and magnetising fields respectively. The latter two are defined by:

$$\mathbf{D} = \epsilon_0 \mathbf{E} + \mathbf{P} \tag{2.9}$$

$$\mathbf{H} = \frac{1}{\mu_0}\mathbf{B} - \mathbf{M} \tag{2.10}$$

Where $\mathbf{P}$ is the polarization field and $\mathbf{M}$ is the magnetisation field, these fields arise due to the bound charges throughout the medium interacting with the EM field.

The force exerted by an optical tweezer can be subdivided into the gradient and scattering components, for most modelling research this is how the force fields are reported. The gradient force is a conservative force brought about by the polarisation of dielectric materials which is directed towards the point of maximum intensity (for a simple Gaussian beam this would be at it's focal point) [2]. Typically, optical tweezers will utilise higher numerical aperture lenses in order to increase the intensity, thus allowing for stronger gradient forces at the trade off of decreased trapping depth.

The scattering force arises from the scattered field of the trapping beam pushing the

target object away from the focal point. While some trapping arrangements can induce transverse scattering forces for simple spheres the scattering force is only significant in the direction of propagation [3] The equilibrium position is found when the gradient force far exceeds both the the scattering force, and the thermal energy of the particle.

2.1.0.1 Harmonic Traps

When a sphere is located at the centre of a laser the gradient force will try to recentre the sphere if it is displaced. If the restoring force is proportional to the sphere's displacement this is referred to as a harmonic trap. The ratio of the restoring force to the displacement is called the trap stiffness (denoted by κ), and is an important characteristic of the trap. Shown below is a typical force displacement curve for a single sphere in a focused Gaussian beam.

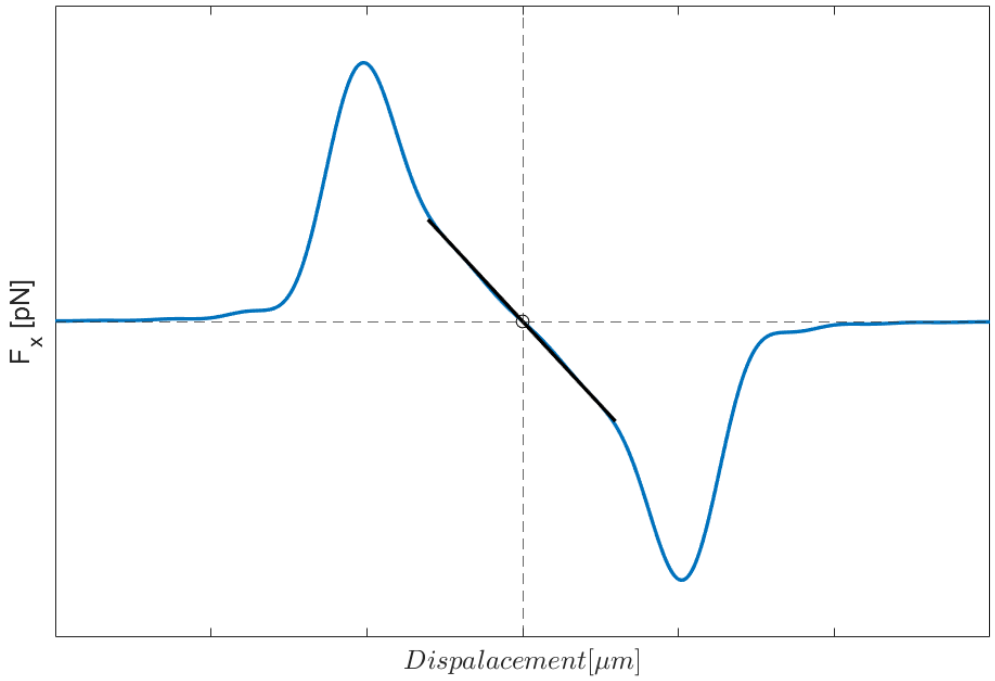

Figure 2.1: Example of a sphere's ($r = 1\ \mu m$) force-displacement curve while moving along the x-axis, where $x = 0$ is the centre of the beam. The harmonic regime is highlight by the black linear fit.

The strength of the optical trap is directly proportional to both the laser power and the contrast in refractive indices between the medium and the particle. Fully describing and calculating the optical forces is dependent on the ratio between the particle size (a) and the trapping wavelength (λ). The scattering theory for computing the optical force is dependent on this ratio.

2.2 Lornez-Mie Theory

The Lorenz-Mie theory provides an exact solution to the Maxwell equations for the scattering caused by an isotropic sphere. This theory describes the scattered wave given off by a dielectric sphere when incident by a plane wave as a summation of partial spherical waves. For any spherical wave the vector fields must solve the Helmholtz wave equation given by:

$$\nabla^2\mathbf{E} + k^2\mathbf{E} = 0 \tag{2.11}$$

Where k is the wave number of the electromagnetic radiation ($k = 2\pi/\lambda$). This combined with the constraints of Maxwell's equations leaves very few exact solutions apart from spherical or planar waves. For a laser of arbitrary shape the electric field can be described as a summation of partial spherical waves multiplied by an expansion coefficient. Depending on the beam in question the expansion coefficients can be tailored to match the desired beam shape. For a Gaussian beam interacting with a particle of volume V, the incident, internal, and scattered fields are given as [4]:

$$\mathbf{E}_{\text{inc}}(\mathbf{r}) = E_0 \sum_{n}^{\infty} \sum_{m=-n}^{n} \left[a_{nm}\mathbf{M}_{nm}^{(1)}(\mathbf{r}) + b_{nm}\mathbf{N}_{nm}^{(1)}(\mathbf{r}) \right] \tag{2.12}$$

$$\mathbf{E}_{\text{int}}(\mathbf{r}) = E_0 \sum_{n}^{\infty} \sum_{m=-n}^{n} \left[d_{nm}\mathbf{N}_{nm}^{(1)}(\mathbf{r}) + c_{nm}\mathbf{M}_{nm}^{(1)}(\mathbf{r}) \right] \tag{2.13}$$

$$\mathbf{E}_{\text{scat}}(\mathbf{r}) = E_0 \sum_{n}^{\infty} \sum_{m=-n}^{n} \left[p_{nm}\mathbf{N}_{nm}^{(3)}(\mathbf{r}) + q_{nm}\mathbf{M}_{nm}^{(3)}(\mathbf{r}) \right] \tag{2.14}$$

where a_{nm}, b_{nm}, c_{nm}, d_{nm}, p_{nm}, and q_{nm} are the expansion coefficients of each of

the fields, and $\mathbf{M}_{nm}$ and $\mathbf{N}_{nm}$ are the magnetic and electric vector spherical harmonics respectively. The superscripts denote whether the field is inward [(1)] or outward propagating [(3)]. By linearity of Maxwell's equations, its possible to relate the expansion coefficients of the scattered field directly to those of the incident field. As such we can write the scattering coefficients in terms of their incident components and the target's 'T-matrix'.

$$\begin{pmatrix} q_{mn} \\ p_{mn} \end{pmatrix} = \mathbf{T} \begin{pmatrix} a_{mn} \\ b_{mn} \end{pmatrix} = \begin{pmatrix} T_{11} & T_{12} \\ T_{21} & T_{22} \end{pmatrix} \begin{pmatrix} a_{mn} \\ b_{mn} \end{pmatrix} \tag{2.15}$$

Where the matrix $\mathbf{T}$ accounts for the targets shape, and refractive index. The T-matrix method can be easily applied to any solution of Maxwell's equations, for example Eq. (2.14) can be instead be rewritten as:

$$\mathbf{E}_{\text{scat}}(\mathbf{r}) = E_0 \sum_{n}^{\infty} \sum_{m=-n}^{n} \begin{pmatrix} T_{11} & T_{12} \\ T_{21} & T_{22} \end{pmatrix} \begin{pmatrix} a_{mn} \\ b_{mn} \end{pmatrix} \begin{pmatrix} \mathbf{N}_{mn}^{(3)} & \mathbf{M}_{mn}^{(3)} \end{pmatrix} \tag{2.16}$$

In order to compute the optical force and torque applied to a given object one simply needs to know the momentum carried by the incident and scattered fields. So long as we know the expansion coefficients of the incident beam we can find the scattered beam coefficients via Eq. (2.15) to compute the force. This project utilises the results from Farsund [5] but in the form used by Crichton [6]. As an example the linear momentum carried by any beam can be computed via:

$$\begin{aligned} \langle P_{z,\ in} \rangle = -\frac{1}{4\pi k^2} \sum_{n,m} \Bigg(& \frac{m}{n(n+1)} \Im[a_{nm} b_{nm}^*] \\ & + \frac{1}{n+1} \left[\frac{n(n+2)(n-m+1)(n+m+1)}{(2n+1)(2n+3)} \right]^{1/2} \\ & \times \Im[b_{nm} b_{nm}^* + a_{nm} a_{n+1m}^*] \Bigg) \end{aligned} \tag{2.17}$$

And the linear momentum carried by the scattered beam is given by:

$$\begin{aligned}\langle P_{z,\ out}\rangle = -\frac{1}{4\pi k^2}\sum_{n,m}\Bigg(&\frac{m}{n(n+1)}\Im[p_{nm}q^*_{nm}]\\ &+\frac{1}{n+1}\left[\frac{n(n+2)(n-m+1)(n+m+1)}{(2n+1)(2n+3)}\right]^{1/2}\\ &\times\Im[q_{nm}q^*_{nm}+p_{nm}p^*_{n+1m}]\Bigg)\end{aligned} \tag{2.18}$$

Therefore the total force imparted to the trapped particle is thus:

$$\boldsymbol{F_z} = \frac{dP}{dt} = P_{z,\ in} - P_{z,\ out} \tag{2.19}$$

Where $a_{nm}, bnm, p_{nm}, \& q_{nm}$ are the beam expansion coefficients used in (2.12) & (2.14). Similar expressions are shown in Sec. 2.6 for calculating the optical torque. Lorenz-Mie theory can be applied to describe the scattering from any particle regardless of size, though as the size of the target particle changes - relative to the wavelength of light - the theory describing the electromagnetic fields are better easier to approximate by alternative theories. When $a \gg \lambda$ the optical force is best described by the Ray-Optics model. In the opposite case the target particle is better approximated as a single electric dipole as described by the Rayleigh approximation.

2.2.1 Ray-Optics Regime

The Ray-Optics model is the simplest to understand, this theory models the electromagnetic field as a collection of individual 'rays' that propagate and are refracted according to Snell's Law. Based on the change in direction momentum is transferred to the target particle; with rays closest to the centre of the beam having greater intensity than those rays at the very edge of the beam. Consider a particle struck by two rays in a Gaussian beam, one coming close to the centre, and the other ray coming from the edge. As each ray is refracted by the target sphere a force is imparted onto it, the total force imparted is given by:

$$F_i = Q_i\frac{\Delta nP_i}{c} \tag{2.20}$$

where Q_i is the trapping efficiency, Δn is the difference in refractive indices between the solution and the target particle, and P_i is the power of the individual ray. The net force can be subdivided into its gradient and scattering components, where the latter directs the particle to the centre of the beam, and the latter acts on the particle in the direction of beam propagation. For a beam with a Gaussian intensity distribution P_i will fall off as you move from the centre of the beam. The ray optics model is ideal when dealing with larger particles whose diameter far exceed the wavelength of light being scattered. While it can be useful in predicting the forces experienced by said particle's it does not fully capture the behaviour of light when considering interference between different rays.

2.2.2 Rayleigh Scattering

The Rayleigh approximation is for describing a particle when $a \ll \lambda$. The underlying theory is that a dielectric sphere can be treated as a dipole while in the presence of the electromagnetic field. In which case the scattering force is given simply by the scattering of the induced dipole, and the gradient force is due to the Lorentz force [7]. The gradient forces in the principle Cartesian axis are described by Harada et al [2] in MKS units as a restorative rectangular force field:

$$F_{grad,x} = -\hat{x}\frac{2\pi n_2 a^3}{c}\left(\frac{m^2-1}{m^2+2}\right)\frac{4\tilde{x}/w_0}{1+(2\tilde{z})^2} \times I(r) \tag{2.21}$$

$$F_{grad,y} = -\hat{y}\frac{2\pi n_2 a^3}{c}\left(\frac{m^2-1}{m^2+2}\right)\frac{4\tilde{y}/w_0}{1+(2\tilde{z})^2} \times I(r) \tag{2.22}$$

$$F_{grad,z} = -\hat{z}\frac{2\pi n_2 a^3}{c}\left(\frac{m^2-1}{m^2+2}\right)\frac{4\tilde{z}/w_0}{1+(2\tilde{z})^2} \times I(r) \times \left[1-\frac{2(\tilde{x}^2+\tilde{y}^2)}{1+(2\tilde{z})^2}\right] \tag{2.23}$$

where:

$$I(r) = \left(\frac{2P}{\pi w_0^2}\right)\frac{1}{1+(2\tilde{z}^2)}\exp\left[-\frac{2(\tilde{x}^2+\tilde{y}^2)}{1+(2\tilde{z})^2}\right] \tag{2.24}$$

Where m is the relative refractive index (n_1/n_2), n_2 is the particle's refractive index, ω_0 is the beam waist, a is the radius of the particle, and $\tilde{x}, \tilde{y}, \tilde{z}$ are simply the x, y, z

coordinates but scaled by the beam radius. The scattering force however, is dependent on the effective scattering cross-sectional area.

$$F_{\text{scat}} = \hat{z}\left(\frac{n_2}{2}\right) C_{pr} I(r) \tag{2.25}$$

where:

$$C_{pr} = \frac{8}{3}\pi(ka)^4 a^2 \left(\frac{m^2-1}{m^2+2}\right)^2 \tag{2.26}$$

There is a clear difference between Eq. (2.21)- (2.24) and Eq. (2.19), namely that the Rayleigh regime is not concerned with the state of the scattered field. This is because if the particle is approximated by a point dipole we can ignore the momentum transfer calculation and simply compute the Lorenz force for a dipole in an electric field. While not important for optical force calculation higher complexity scattering problems can be simplified by subdividing the particle into discrete dipoles (see Sec 2.3), in which case the scattered field is now significant. As the target particle gets larger this assumption fails to accurately describe the trapping force [8]. For larger particles the optical force and scattering is better described via the Lorenz-Mie theory.

2.3 Scattering methods

There are several methods available to calculate the scattered field produced by a particle. While one can compute this by directly applying Lorenz-Mie theory, describing the interactions between focused beams and complicated shapes can be computationally slow and memory intensive. As a result, several alternative scattering approaches have been developed that allow for faster computation times simplifying the scattering problem.

2.3.1 T-matrix Method

The T-matrix method was first developed by Peter Waterman with his research into acoustic wave scattering [9], this would later be extended to electromagnetic waves. Sometimes referred to as the extended boundary condition method (ECBM), the method

replaces the scatterer with a series of surface currents over the targets surface. These currents are chosen so that the electromagnetic field outside is identical to the original problem [10]. By expanding the fields one can derive the individual elements of **T** until a desired accuracy is achieved.

For this project we utilised an extension of the ECBM known as multi-sphere T-matrix method (*mstm*). Developed by Mackowski [11] the computational code computes the scattered field from each sphere within the target cluster and the incident field itself. The scattering between spheres will converge to a final result but modern codes truncate the calculations to an upper number of iterations (denoted by N_{max}) to fit a desired accuracy and computational time. By centring the expansion at the origin of each sphere the individual sphere T-matrices can be computed, then using the addition theorem, the target centred T-matrix is computed.

The T-matrix method is exceptionally useful for computing the scattering from any arbitrary spherical aggregate. However, the T-matrix method by itself can be computationally taxing as the number of spheres increases [11]. While it is possible to solve for the full electromagnetic field of each the entire cluster this is only applicable for a single orientation and can be even slower for large aggregates [12], [13]. The benefit of *mstm* is that the major scattering properties (scattering and extinction cross sections, scattering matrices, etc) can all be computed both for single orientations, or averaged over multiple orientations to determine the average scattering from the target particle.

2.3.2 Discrete Dipole Approximation

The discrete dipole approximation (DDA) is a general method that can be applied to the scattering from particles of arbitrary composition and geometry. Developed by Purcell and Pennypacker [14], the DDA method approximates the particle as being constructed of discrete dipoles. Each dipole interacts with both the incident field and the scattered fields from every other dipole surrounding it. The resulting scattered field is identical to the scattered field produced by direct integration of Eq. (2.13) throughout the full particle volume [15]. The integral form for the total electric field inside a scatterer is

given as [10]:

$$\mathbf{E}(\mathbf{r}) = \mathbf{E}_{inc}(r) + \sum_{i}^{N_d} \mathbf{E}_{scat,i} = \mathbf{E}_{inc}(r) + \int_{V/V_0} d^3 r \bar{\mathbf{G}}(\mathbf{r}, \mathbf{r}') \chi(\mathbf{r}') \mathbf{E}(\mathbf{r}') \tag{2.27}$$

Where $\bar{\mathbf{G}}$ is the Greens dyadic function of free space, which defines the impulse response between two separate dipoles; and χ is the susceptibility of the medium, which describes the degree of polarisation of the medium in the presence of an electric field. One of the primary advantages of DDA over the T-matrix method is that the composition of the target can be changed freely. When comparing different computational scattering methods, the ECBM was found to be better suited for simulating the scattering of symmetric targets as the ECBM can use the target's symmetry to speed up calculations [10]. But when dealing with inhomogeneous media DDA is more efficient compared to ECBM.

The DDA method can be used to derive the target's T-matrix. After generating the far field expansion of the electric field (Eq. (2.27)), the vector spherical expansion far field (Eq. (2.14)) can be matched to it. Solving for the expansion coefficients p_{nm}, and q_{nm} allows one to construct the T-matrix of the target.

2.4 Langevin Equation

Describing any microscopic motion requires an understanding of a molecules diffusive behaviour, for the case of optical tweezers the most complete model of diffusion is the Langevin equation. Models such as the Fickian, and Einstein derivations are sufficient for macroscopic behaviours the Langevin equation better describes the microscopic characteristics of any diffusive behaviour.

The Fickian model describes the net flux of solute molecules into a finite volume of fluid being proportional to the density gradient $\delta\rho(u,t)/\delta u$ [16]. It assumes that the solute molecules do not collide with one another or with molecules in the solution; overall, the Fickian model is used to describe how solute molecules disperse over long periods of time. It does not provide any incite into the forces acting on individual

molecules, whereas the Langevin model captures the physical interactions between an individual molecule and the surrounding fluid over a wide range of time scales.

The Einstein model of diffusion expands upon the Fickian model by considering the collisions between individual molecules. If we consider a single particle suspended in a solution it will experience multiple collisions with other molecules [17] over a given time interval δt. The Einstein molecule allows us to consider how individual molecules behave while suspended in a surrounding fluid. Where it begins to falter is when we consider bringing δt to 0; in this scenario the molecule experiences not many but only individual collisions. The Einstein model does not consider the inertia of the molecule in question and so for very short time frames the model implies that the molecule's velocity changes instantly after each collision [17], [18]. Furthermore, the kinetic energy of each collision is not limited by the thermal energy of the system, meaning that using the Einstein model to predict a particle's trajectory to an finite degree of accuracy implies that the particle has infinite kinetic energy [18]. This failure to describe motion over smaller time frames is addressed in the Langevin model by accounting for the fluid drag of the system, where any sudden change in velocity must result in a proportionally opposed drag force [19].

The Langevin model of diffusion assumes that the net force on a particular particle is described fully by these individual collisions [19]. Unlike the Fickian model it provides a full description of the interactions between the target molecule and the surrounding fluid; while also being able to describe its motion over any time scale, unlike the Einstein model:

$$m\frac{dv}{dt} + \gamma_0 v + F(t) = W(t) \tag{2.28}$$

Where the first term accounts for inertial forces, the second term accounts for friction forces which counteract the particles current motion (γ_0 is the friction coefficient), and the final term accounts for the random Brownian force. The $F(t)$ is there for convention which accounts for any external forces acting on the particle. These three terms are equal to the random Brownian motion of the surrounding fluid. We can say

that the noise term $W(t)$ has a normal distribution, being scaled by the thermal energy of the system, with a correlation function of:

$$W(t) = \sqrt{2k_B T\gamma_0}\eta(t) \tag{2.29}$$

$$\langle W_i(t)W_j(t')\rangle = 2k_B T\gamma_0\delta(t-t') \tag{2.30}$$

The Langevin model can be extrapolated to describe the diffusive behaviour of an overall system, but for this project we can instead consider the behaviour of some particle with a diffusion tensor D suspended in a viscous fluid and spacially localised by an optical potential with trap strength κ. Assuming the only external force acting on our particle is the laser, the net force should be exactly equal to force of the stochastic collisions due to the fluids thermal energy. If we focus our analysis when the particle is stably trapped and assume that the trap is harmonic, we can model the trapping force as a Hookean spring ($F(t) \approx \kappa x(t)$). The full Langevin equation for an optically trapped particle is therefore given as:

$$m\frac{\delta^2 x(t)}{\delta t^2} + \gamma_0\frac{\delta x(t)}{\delta t} + \kappa_x x(t) = \sqrt{2k_B T}\eta(t) \tag{2.31}$$

(2.31) provides an accurate description of strongly trapped particles. Despite this the analytical solution of the Langevin equation requires integration of the noise term making it difficult to simulate the trajectory of a given particle [20]. Instead, it is often far easier to solve the equation numerically and use the analytical solution to calibrate and extract information about the particle and fluid, and how the two interact with the optical trap.

2.4.1 Finite Difference

The Finite Difference approach involves discretizing the time and spatial elements in order to approximate the higher order terms. If we assume that $x(t)$ is differentiable

to n (we can find its n^{th} derivative) then we can use the Taylor series expansion to get:

$$x(t+\Delta t) = x(t) + \frac{x'(t)}{1!}\Delta t + \frac{x^2(t)}{2!}\Delta t^2 + ... + \frac{x^n(t)}{n!}\Delta t^n + R_n(x(t)) \tag{2.32}$$

Where $R_n(x(t))$ is the remainder term between the Taylor expansion to term n and the actual expression. If we limit our approach to the first derivative only, we find that for sufficiently small values of R_1 the velocity and acceleration can be approximated as:

$$x'(t) \approx \frac{x(t+\Delta t) - x(t)}{\Delta t} \tag{2.33}$$

$$x''(t) \approx \frac{x'(t+\Delta t) - x'(t)}{\Delta t} = \frac{x(t) - 2x(t+\Delta t) + x(t+2\Delta t)}{\Delta t^2} \tag{2.34}$$

By reversing the time step (i.e. use $-\Delta t$) to approximate the velocity and acceleration based on the previous time steps, we can discretise the position by taking finitely small time steps (i.e. $x(t) = x_i,\ x(t-\Delta t) = x_{i-1}$). The same cannot be done for noise, as no information is known about $W(t)$ at any time. We can instead say that the velocity of a Brownian particle should approximate our noise as a random walk, where at each new time step, the position changes randomly within a given range. Constricting the variance to $\sqrt{2D}/\Delta t$ allows us to represent the noise using the finite-difference approach as:

$$m\frac{x_i - 2x_{i-1} + x_{i-2}}{\Delta t^2} = -\gamma\frac{x_i - x_{i-1}}{\Delta t} + \sqrt{2k_BT\gamma}\frac{w_i}{\sqrt{\Delta t}} \tag{2.35}$$

Where w_i is a random real number between -1 and 1, we can say that it is normally distributed around 0 for simulation purposes. We can rearrange this for x_i to approximate the Brownian motion of a particle (setting $x_0 = 0$), where the characteristic time is $\tau = m/\gamma$. Now in the case of an optical trap, the restoration time scale is given by $\tau_{OT} = \kappa_x/\gamma$ which for strongly trapped particles is far greater than the characteristic time. Therefore for simulation purposes, we can neglect the particle's inertia which

allows the motion of an optically trapped particle to be written as:

$$x_i = x_{i-1} - \tau_{OT}\ x_{i-1}\Delta t + \sqrt{2D\Delta t}\ w_i \tag{2.36}$$

This result can be generalised for a 3-dimensional description of an optically trapped particle, where each Cartesian direction has its own unique characteristic restoration time. We see from the result that trajectory is dependent on only a handful of factors, the trap stiffness κ_x, the fluid viscosity γ, and the thermal energy of the system k_BT (with the latter two being related by Einstein's formulation of the diffusion coefficient $D = k_BT/\gamma$). Therefore, by calculating these parameters to a high degree of precision allows one to get a precise description of the forces experienced by a target particle, which in the past has been used for highly accurate force transduction [21], [22].

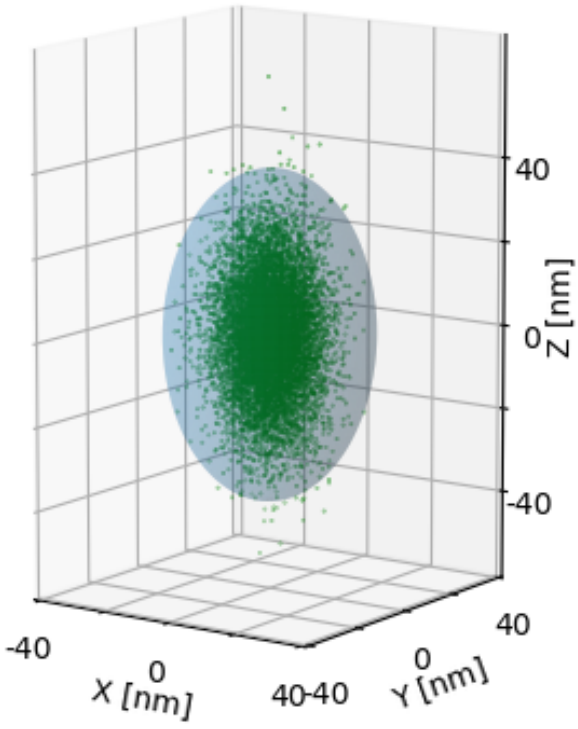

Figure 2.2: Example trajectory created using Finite Differences method for a $2\mu m$ diameter sphere. Trap stiffness's were estimated using *ott* at $\kappa_x = \kappa_y = -100\ pN/\mu m$ and $\kappa_z = -25\ pN/\mu m$. The particle's motion can be localised around the shaded ellipsoid.

2.5 Calibration Techniques

There are several approaches for calibrating and characterizing the optical trap, each approach has its drawbacks and benefits so each option should be chosen based on what elements want to be characterized. The basis for each of these methods stems from the analytical solution of the Langevin equation:

$$x(t) = x(0)e^{-t/\tau_{OT}} + \sqrt{2D}\int_0^t dsW_x(s)e^{-(t-s)/\tau_{OT}} \tag{2.37}$$

Positional data is often acquired in an experimental setting either using image analysis or photodiodes to infer the particles position relative to the beam focus. The former is often used in cases when precision is not a key concern, as often a standard CCD camera will have limited spacial and temporal resolution. The latter method often requires the use of a quadrant photo diode(QPD), the data provided by the QPD will often need to be converted to physical units to compute the force directly - see Eq. (2.50).

2.5.1 Potential Well Analysis

The Langevin equation for an optically trapped assumes that the trap acts similar to a Hookean spring that creates a potential well about its centre. Therefore a simple analysis method is to understand the height and width of said potential well.

Potential analysis is a useful technique for estimating the strength of an optical trap; this method assumes that the force acting on the particle is purely conservative, an accurate presupposition if we ignore the motion of the particle as it enters the trap. This is because the scattering force is far more significant far away from the potential well and is negligible if the trap strength is much greater than the thermal fluctuations. With this in mind we can write the probability of finding the particle at position x as:

$$\frac{\rho(x)}{\rho_0} = e^{-\frac{U(x)}{k_B T}} \tag{2.38}$$

which therefore means we can write the potential well as:

$$U(x) = -k_B T \; ln\left(\frac{\rho(x)}{\rho_0}\right) \tag{2.39}$$

Now assuming our laser acts as a Gaussian beam we should be able to describe the probability distribution $\rho(x)$ centred at some equilibrium position x_0:

$$\rho(x) = \sqrt{\frac{\kappa_x}{2\pi k_B T}} exp\left(-\frac{\kappa_x}{2k_B T}(x - x_{eq})^2\right) \tag{2.40}$$

By inserting (2.40) into (2.39) we can fit the potential well in order to determine the trap strength κ_x, and an estimation of the equilibrium position x_{eq}. This has some limitations in that the large fluctuations can throw off the fit meaning a longer acquisition time is necessary to properly fit the potential well, making it difficult to characterise weakly trapped particles who may not remain trapped for long. It also provides no information on the particle itself (i.e. the friction coefficient γ and diffusion coefficient D).

2.5.2 Equipartition method

The Equipartition method is by far the fastest and simplest means for estimating the trap strength but unlike Potential Analysis is limited strictly to harmonic potentials. This can be often not the case for highly focused beams, as the trap strength can vary due to polarisation differences. Simply put we can use the equipartition theorem to relate the potential well to the particle's thermal energy using (2.40):

$$\langle U(x) \rangle = \frac{1}{2}\kappa_x \left\langle (x - x_{eq})^2 \right\rangle = \int_{-\infty}^{\infty} \rho(x)(x - x_{eq})^2 = \frac{1}{2} k_B T \tag{2.41}$$

$$\implies \kappa_x = \frac{k_B T}{\langle (x - x_{eq})^2 \rangle} \tag{2.42}$$

By taking a time average over multiple trajectories to get $\langle x - x_{eq} \rangle$ we can get a fairly accurate estimation of the trap strength. Because of this requires a time average of the particle's displacement any large errors in the position measurement can have knock-on effects. Likewise with the potential analysis route, no information is gleaned

about the particle itself.

2.5.3 Mean Square Displacement

Mean square displacement (MSD) is a common means of describing the random motion of a given particle (or group of particles). This is useful information if say for example we want to understand reaction kinetics on the surface of a catalyst, if we know how far its likely to move from the surface we can tell if its likely to react when a catalytic site becomes available. As it pertains to colloids, consider a suspension of silica spheres immersed in a fluid undergoing Brownian motion (as described by the Langevin Equation) so that:

$$mx''(t) + \gamma x'(t) = \eta(t) \tag{2.43}$$

Where γ is the objects friction coefficient which for spheres is given as $\gamma = 6\pi\eta r$, and $\eta(t)$ is a random white noise variable that is directly related to the thermal energy of the surrounding fluid. If the motion is truly random then we should see an average displacement of 0 regardless of how long we measure for. If we wish to understand the effects of a given external factor (i.e. an electric field or localised heating), simply looking at displacement will reveal nothing of value as its difficult to differentiate between diffusive and a biased motion.

For each sphere we can record its position in the $x - y$ plane and measure its displacement from a set reference point; for example with an optical tweezer this could be the beam focus. We can measure the MSD by forming a 'window' between two points in time of the trajectory (i.e. $t\&t + \tau$) and sliding this window along the entire trajectory length - to eliminate -ve displacements we take the square - we can then take the average of this series. Repeating over a range of time lags allows us to describe the MSD as a function of τ:

$$MSD(\tau) = \left\langle |x(t+\tau) - x(t)|^2 \right\rangle \tag{2.44}$$

If we use (2.37) for an optical tweezer we can expand out the squared term to get

an analytical expression for the MSD as a function of time lags:

$$MSD(\tau) = \left\langle |x(t+\tau)^2 - 2x(t+\tau)x(t) + x(t)^2| \right\rangle = \frac{2k_BT}{\kappa_x}\left[1 - e^{-\frac{\tau}{\tau_{OT}}}\right] \tag{2.45}$$

From this expression its evident that the mean squared displacement increases with larger values of τ until it reaches a maximum value as shown below by the dotted line.

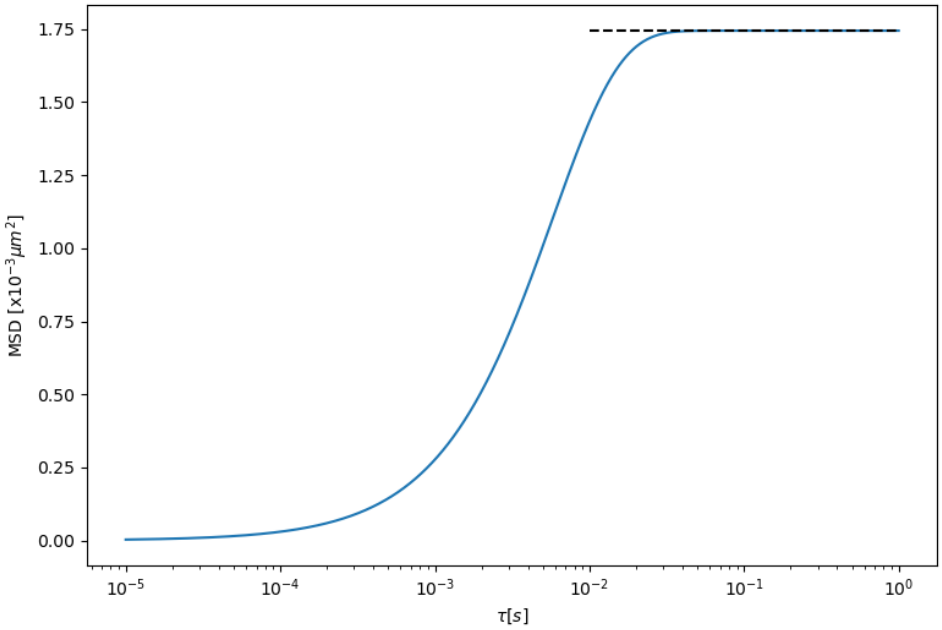

Figure 2.3: Example mean squared displacement using (2.45), for a $1\mu m$ sphere trapped by an optical potential well. The dotted line represents the upper limit of the sphere's displacement due to the optical trap.

The MSD plot can be subdivided into two regimes, when $\tau \gg \tau_{OT}$ the particle is experiencing the harmonic potential described by the equipartition theorem, and when $\tau \ll \tau OT$ the particle is said to be freely diffusing within the trap focus. Of course for a freely diffusing object the MSD will never reach a plateau value, comparing MSD's for different particles provides a simple visual indicator of the difference in trapping strength. The MSD method is an already very versatile analytical tool for diffusive

motion, however it is rather slow in computing time meaning it is only really beneficial when a high degree of accuracy is required and shorter time resolutions are unavailable - such as using a quadrant photo diode instead or a high speed CCD.

2.5.3.1 Angular Mean Square Displacement (MSAD)

It is also possible to plot the angular MSD (MSAD) using simulative data, however using this to describe the torque acting on an asymmetric object is difficult due to fact there is no simple approximation of the rotational stiffness. Vigilante *et al* [23] derived the upper limit of a dimer's MSAD along its long axis by assuming it was strongly trapped and so had limited angular motion, there expression gives:

$$\lim_{\tau\to\infty}\left\langle(\Delta u_z)^2\right\rangle = 2\left[1-\frac{1}{4\beta\kappa_r}\left(\frac{exp(\beta\kappa_r)-1}{exp(\beta\kappa_r)F(\sqrt{\beta\kappa_r})}\right)^2\right] \tag{2.46}$$

Where, u_z is the unit vector connecting the two spheres of the dimer, $\beta = 1/k_BT$, κ_r is the rotational stiffness of the trap, and F is Dawson's integral [24]. Vigilante's paper expressed that they couldn't compute $MSD(\tau)$ because they couldn't solve the Einstein-Smoluchowski equation which describes the diffusion constant for dielectric particles. This would require a full description of a particle's electrical mobility and charge distribution - the latter could be achieved via a discrete dipole approximation, the former would be dependent on both the particle's position and relative orientation to the electric field.

2.5.4 Power Spectrum Density (PSD)

The power spectral density (PSD) method is by far the most versatile method for observing the dynamics of any object within an optical trap, allowing for fast calibration times while also quickly filtering out typical noise sources. After recording a trajectory over some time t_{msr}, taking the Fourier transform of a particle's trajectory yields:

$$\hat{x}(f) = \frac{(2D)^{1/2}\hat{\eta}}{2\pi(f_c - if)} \tag{2.47}$$

where x can either be the physical position (relative to the trap focus) or a recorded signal from a position-detector,and $\hat{\eta}$ is the Fourier transform of the white noise (see Eq. (2.54)). Where the values are exponentially distributed as opposed to being normally distributed in the time domain [21]. We can therefore ignore the white noise from our analysis by looking at the spectral density of $\hat{x}(f)$ that produces a Lorentzian curve:

$$S_x = \frac{\hat{x}^2}{t_{msr}} = \frac{D}{2\pi(f_c^2 + f^2)} \tag{2.48}$$

Eq. (2.48) can be fitted via a simplified geometric series $S_x = 1/(A + Bf_k^2)$ which allows us to compute both the diffusion coefficient (in arbitrary units) and the corner frequency f_c which is directly related to the trap strength via $f_c = \kappa_x/(2\pi\gamma)$. The Lorentzian shape implies that the trap is harmonic - but not symmetric - which assumes that the particle itself is an isotropic scatterer. Anisotropic scatterers can produce an Lorentzian curve if the angular component of the power spectra is insignificant. The magnitude of rotational motion (whether it is stochastic [25] or periodic [26]) will effect how drastically it departs from a typical Lorentzian curve.

Like with the analytical expression of the mean squared displacement we see two distinct regions, when $f \ll f_c$ the PSD reaches a plateau value that when converted to length units represents the maximum displacement the particle can move beyond the focus. When $f \gg f_c$ the PSD falls off exponentially which denotes the particle is freely diffusing within the beam focus.

The Lorentzian relationship is only valid for frequency terms up to the Nyquist frequency (half of our sampling rate), this is because we are only taking a finite sampling of the particle's trajectory meaning the signal is aliased. Berg and Sorensen provide a suitable modified Lorentzian to account for the aliasing effects [21]:

$$S_x = \frac{(\Delta x)^2 \Delta t}{1 + c^2 - 2c\cos 2\pi f_k \Delta t/N} \tag{2.49}$$

Where N is the total number of samples taken, Δx & c have no direct physical interpretation and are defined in [21]. Further modifications can be made to the power

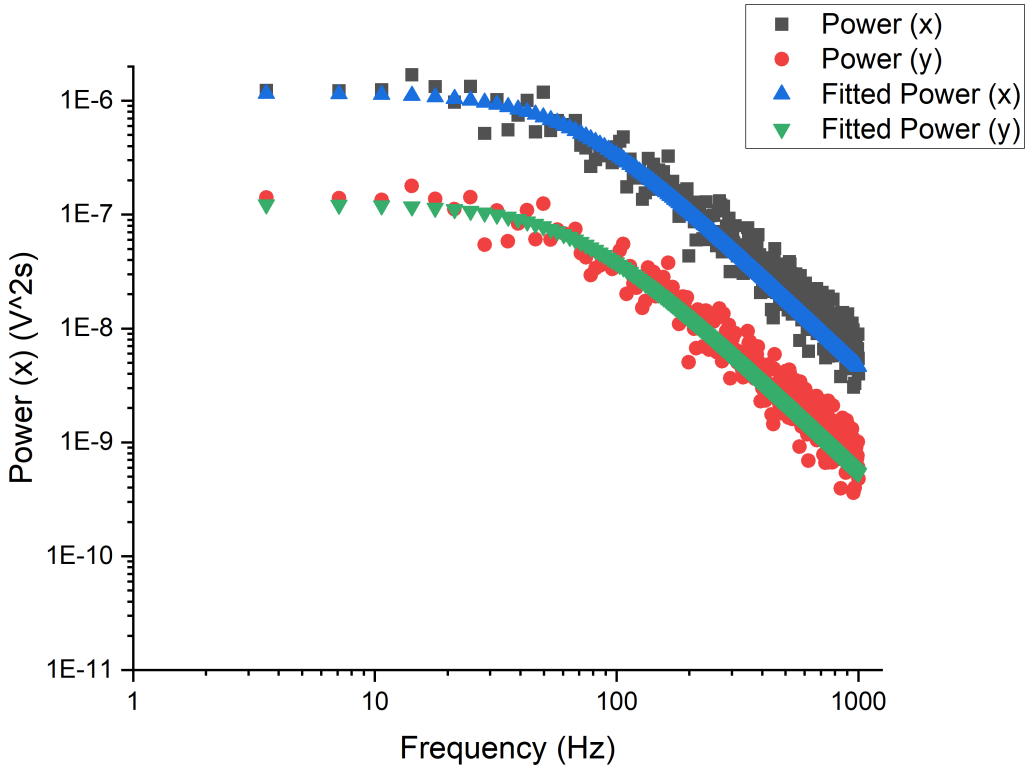

Figure 2.4: Example PSD fitted using (2.48), power spectra is collected from an optically trapped silica sphere suspended in water. The difference in magnitude is due to the asymmetry of the quadrant photo diode having a stronger signal response in the direction of the polarisation vector. Using a correction factor (see (**??**)) will adjust the power spectra to better describe the trap shape.

spectrum model but this is only useful when a high degree of accuracy is necessary. Typically power spectra are recorded using a Quadrant Photo Diode (QPD), which records motion in voltage units, not in units of length. There are two main methods for converting to physical units: If multiple photodetectors are available then a differential interference contrast (DIC) system can be used to compute the linear relationship between the beads displacement and the photodiodes signal [3]. While this is useful when high force precision is necessary it also allows you to collect information about the particle's motion along a single direction, making it ideal for less focused beams. Alternatively, if the size distribution is very wide but each particle can be accurately sized, then a conversion factor can be approximated by comparing the fitted value of

the diffusion coefficient, and the reported value given by the Stokes-Einstein relation.

$$D_{SE} = \frac{k_B T}{\gamma_0} \Rightarrow Conversion\ Factor\ [m/V] = \sqrt{\frac{D_{SE}}{D_{fit}}} \tag{2.50}$$

With the latter method, the local fluid viscosity must be known to a high degree of accuracy, depending on the local heating effect this may be as trivial increase or it may be significant enough to drastically alter the characterisation. PSD analysis is often seen as the gold standard for calibration as it can be fine tuned to the point that optical forces can be computed on the order of $10^{-15}N$ [21], it captures all of the information acquired by other calibration techniques while filtering out noise and requiring a relatively small amount of data collected.

2.5.4.1 Power spectral analysis for rotating objects

The scattering from rotating objects can be partially characterised via the power spectrum density method. Typically papers reporting on the rotation rate of a trapped object will collect a power spectrum and look at the maximum frequency term to determine its rotation rate. However this often neglects any information on the trapping forces acting on particle and only looks at the torque applying around one of the particle's primary axis. There has only been one notable effort to fully characterise the full trapping dynamics on a rotating body, [26] developed a theoretical model for that relates the power spectrum to both the rotational and translational motion simultaneously.

2.6 Simulation of spherical aggregates

Later chapters cover the dynamics of spherical aggregates and anisotropic scatterers, these subjects are particularly difficult to characterise using conventional calibration techniques [27], [28]. As an example consider a symmetric dimer as a paradigmatic aggregate; if we consider the Langevin equation for such a aggregate within an optical

trap we have:

$$\frac{d\vec{r}(t)}{dt} = \frac{\vec{\kappa}_x}{\gamma}\vec{r}(t) + \sqrt{2\vec{D}_x}\eta(t) \tag{2.51}$$

Where $x(t)$ is replaced with $\vec{r}(t)$ to signify that the translational motion is generalised to a 3 dimensional case. Except now, the dimer is undergoing random rotational motion in addition to its Brownian translational motion the first term on the right hand side is no longer purely a function of the dimer's position but also on its orientation. The rotational form of the Langevin equation for a dipole within an external potential is given as:

$$\frac{d\vec{u}(t)}{dt} = \frac{\mu}{\gamma_R}\left[\vec{u}(t) \times E(t)\right] \times \vec{u}(t) + \sqrt{2\vec{D}_R}\lambda(t) \times \vec{u}(t) \tag{2.52}$$

Where $\vec{u}(t)$ is the unit vector aligned along the centres of the two spheres, μ is its dipole moment, and γ_R is the rotational friction coefficient which is given as $\gamma_R = 8\pi\eta r^3$ for a sphere, if the dimer is within a harmonic potential we can write the first term on the right hand side as $\frac{\vec{\kappa}_u}{\gamma} \times \vec{u}(t)$, where $\vec{\kappa}_u$ is the rotational stiffness vector. $\lambda(t)$ is the Brownian rotations from the surrounding fluid, like in the translational case the Brownian rotations are normally distributed and are also uncorrelated so that:

$$\left\langle \lambda(t)\lambda(t') \right\rangle = \delta_{ij}\delta(t - t') \tag{2.53}$$

For an asymmetric scatterer whose radius is comparable to that of the electric field's wavelength we now have a system of simultaneous equations:

$$\frac{d\vec{r}(t)}{dt} = \frac{\vec{\kappa}_x(\vec{u}(t))}{\gamma}\vec{r}(t) + \sqrt{2D}\eta(t) \tag{2.54}$$

$$\frac{d\vec{u}(t)}{dt} = \frac{\vec{\kappa}_u(\vec{r}(t))}{\gamma_R} \times \vec{u}(t) + \sqrt{2\vec{D}_R}\lambda(t) \times \vec{u}(t) \tag{2.55}$$

Fortunately, we do not need to solve these directly as the latter two random variables can be easily approximated if the thermal energy of the system is known, and the rate of change can be assumed as linear if we take a sufficiently small time step that

$\Delta t \ll \kappa_x/\gamma$ & $\Delta t \ll \kappa_u/\gamma_R$. In doing so we now only need to compute the optical force and torque applied to th dimer.

Using a MATLAB package called *Optical Tweezer Toolbox* or *ott* [29] we can compute the beam shape coefficients (a_{nm} & b_{nm}) for any desired beam type. Using the results from [5] we can then compute both the optical force and torque using the beam coefficients and the scattering coefficients (q_{nm} & p_{nm}) which are found by calculating the dimer's T-matrix via *mstm* [11] and then using (2.15). The total force in along the z-direction and the total torque about the z-axis are provided:

$$\begin{aligned}\mathbf{F_z} = -\frac{1}{4\pi k^2}\sum_{n,m}\Bigg(&\frac{m}{n(n+1)}\Im[a_{nm}b_{nm}^* - p_{nm}q_{nm}^*] \\ &+ \frac{1}{n+1}\left[\frac{n(n+2)(n-m+1)(n+m+1)}{(2n+1)(2n+3)}\right]^{1/2} \\ &\times\Im[b_{nm}b_{nm}^* + a_{nm}a_{n+1m}^* - q_{nm}q_{nm}^* + p_{nm}p_{n+1m}^*]\Bigg)\end{aligned} \tag{2.56}$$

$$\begin{aligned}\mathbf{T_z} = -\frac{1}{8\pi k^3}\sum_{n,m}\Bigg(&\frac{m}{n(n+1)}[|a_{nm}|^2 + |b_{nm}|^2 - |p_{nm}|^2 - |q_{nm}|^2] \\ &+ \frac{2}{n+1}\left[\frac{n(n+2)(n-m+1)(n+m+1)}{(2n+1)(2n+3)}\right]^{1/2} \\ &\times\Re[b_{nm}a_{nm}^* + a_{nm}b_{n+1m}^* - p_{nm}q_{nm}^* + q_{nm}p_{n+1m}^*]\Bigg)\end{aligned} \tag{2.57}$$

where a_{nm}, b_{nm}, p_{nm}, and q_{nm} are the beam coefficients of the incident and scattered fields respectively. We can get the x and y force and torque components in a similar form by applying a simple rotation transformation. With the optical forces and torques computed all that remains is to compute the Brownian forces and torques which are constrained by the relation.

$$\langle q_i q_j \rangle = 2D_{ij}\Delta t \tag{2.58}$$

Vigilante et al compiled together a python package that combines both *ott* and *mstm* to simulate the behaviour of spherical aggregates within a predefined optical trap [23]. Now *ott* does have inbuilt T-matrix modules that can be used to model the scattering from different shaped particles; however, for aggregates of spheres the

resultant force is nonsensical (see Chapter 4 for further details). As such we rely on the *mstm* for simulating dimers.

2.6.1 Simulation reference frame

Throughout this project we use the work of Vigilante to perform a systematic study of the dynamics demonstrated by asymmetric dimers in both plane and circularly polarised light. The simulations have two primary frames of reference that require explanation. Firstly, there is the laboratory frame which describes the coordinate system, we define the origin of our simulation as the focus of our trapping beam. While the choice in direction for the x and y axis are arbitrary the z axis is specifically chosen so that it is aligned with the direction of beam propagation.

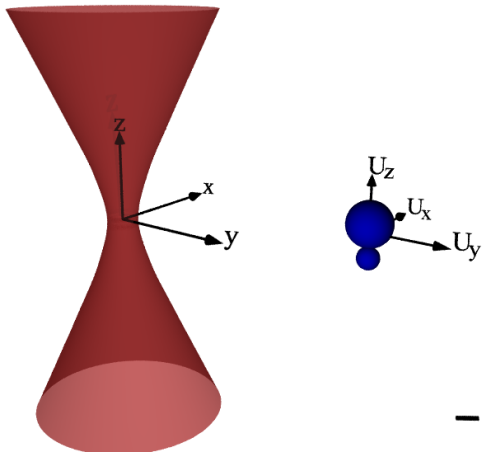

Figure 2.5: Ray scattering render of both the laboratory frame and particle frame for a dimer and a Gaussian beam. The origin of the laboratory frame is defined as the focus of the trapping beam, with the positive z-axis being aligned with the direction of beam propagation. The particle frame is centred on the dimer's centre of mass with the primary axis U_z being aligned with the centres of the two spheres. Black line is scaled to represent 1 μm.

Secondly there is the particle frame which describes the orientation state of the particle, orientations are reported as quaternions which can be readily transformed into rotation matrices. The matrix describes the direction of the particles 3 orientation axis U_x, U_y, and U_z. The latter is oriented so that it is collinear with the centres of

the two spheres; the direction of vector U_z is such that it goes from the centre of a_{II} to the centre of a_I. The origin of the 3 axis' is set on the particle's centre of mass, this is also used to define it's displacement from the origin of the laboratory frame. The diffusion tensor of the dimer is more complex than a sphere's as we must consider the rotational effects experienced by the dimer. We use the analytical solution of Nir & Acrivos [30], where they provided the solution coefficients depending on the dimer's size ratio (a_I/a_{II}). Rather than recalculate the coefficients for every possible configuration of dimer we use a spline fitting function to approximate the diffusion tensor.

2.7 Simulated Quadrant Photodiode

Beyond merely simulating the forces experienced by a spherical aggregate we also developed a simulative quadrant photo diode to replicate the results from a typical calibration test. This builds upon the work from [31] which applied Lorenz-Mie theory to replicate the response signal of a QPD being used in back focal-plane interferometry. Rather than be constrained to individual spheres we can now consider the expected response from any type of spherical aggregate.

In order to simulate a typical experimental set up with a QPD installed as a position detection system we need to evaluate the total magnitude of the electric field incident on the photo-diode surface. While trapping a micro-particle, the scattered and incident fields combine together and interfere with one another. These fields are collected by a condenser lens in the far field limit and are focused onto the QPD surface, the total intensity can be evaluated as:

$$I(x,y) = \epsilon_0 c \left| \begin{bmatrix} E_{i,x}(x,y) + E_{s,x}(x,y) \\ E_{i,y}(x,y) + E_{s,y}(x,y) \\ E_{i,z}(x,y) + E_{s,z}(x,y) \end{bmatrix} \right|^2 \times step(NA_c - \sqrt{x^2+y^2}) \tag{2.59}$$

The last term is simply a representative step term that defines the outer limit by which we evaluate the electric field, this is analogous to our condenser lens removing noise from other light sources by only accepting light at a specific acceptance angle

defined by its numerical aperture NA_c. Depending on the relative size of our particle we can adjust the acceptance angle, this has very little effect on the transverse signals, but for axial evaluations of a trapped particle the numerical aperture should be tuned so that the resultant response curve has negative slope in order to allow for axial position detection, the method for finding this angle θ_Θ is discussed in [32].

The incident beam is simple enough to define given our set up parameters, for the sake of simplicity we assume that our beam is a Laguerre-Gaussian beam of mode $[0.0, 0.0]$ (which is simply a pure Gaussian beam). *Ott* uses a point matching approach to approximate the beam shape coefficients of the incident field by fitting it to the far field estimate. From the QPD's perspective it is receiving light both from the incident and scattered beam simultaneously, as such both fields must be expressed using outgoing vector spherical harmonics.

$$E_{\text{inc}}(r) = E_0 \sum_{nm}^{\infty} \left[a_{mn} \mathbf{M}_{nm}^{(2)}(\mathbf{r}) + b_{nm} \mathbf{N}_{nm}^{(2)}(\mathbf{r}) \right] \tag{2.60}$$

$$E_{\text{scat}}(r) = E_0 \sum_{n=1}^{\infty} i^n \frac{2n+1}{n(n+1)} \left[-ip_{nm} \mathbf{N}_{nm}^{(2)}(\mathbf{r}) + q_{nm} \mathbf{M}_{nm}^{(2)}(\mathbf{r}) \right] \tag{2.61}$$

We can, if we want, further restrict the incident beam by setting the truncation angle to match our microscope object, this applies a hard cut off to the incident beam to better represent experimental conditions. In order to compute the scattering from the target particle *ott* uses the T-matrix method, this is not essential for a simple sphere but is essential for complex shaped particles such as dimers. The matrix from mstm needs to be repackaged to work with the *ott* software, converting it from a column vector into a system of sub matrices.

The scattered and incident fields are then combined together in the far field to get

$I(x, y)$, the quadrant and overall signals are calculated via:

$$Q_i = \sum_{n,m} I(x_{i,n}, y_{i,m}) \tag{2.62}$$

$$S_x = \frac{(Q_1 + Q_2) - (Q_3 + Q_4)}{\sum I_0(x, y)} \tag{2.63}$$

$$S_y = \frac{(Q_1 + Q_3) - (Q_2 + Q_4)}{\sum I_0(x, y)} \tag{2.64}$$

$$S_z = \frac{(Q_1 + Q_2 + Q_3 + Q_4}{\sum I_0(x, y)} \tag{2.65}$$

Where the denominator is the total intensity on the QPD while there is no particle within the trap. The QPD sensitivity is dependent on both the polarisation of the incident beam and the displacement of the target sphere, this is shown in fig. 2.6.

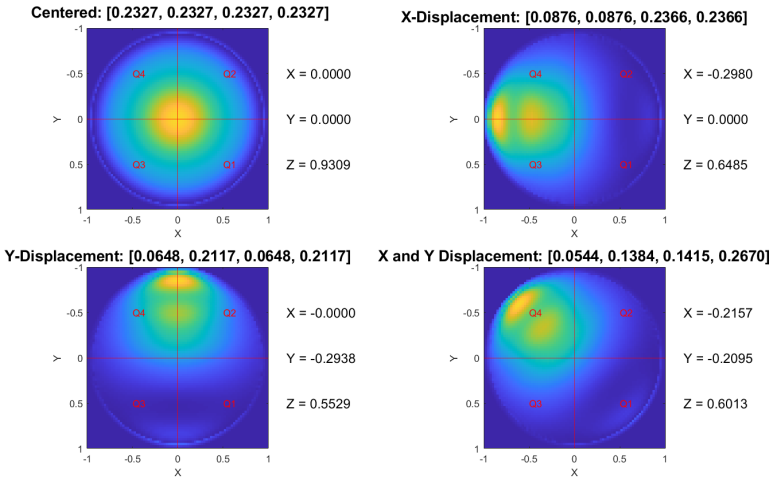

Figure 2.6: Total Field incident on the quadrant photo diode for a several different displacements. Top Left: $2\mu m$ diameter silica sphere placed at the focus of a beam. Top Right: silica sphere is now displaced by $1\mu m$ along the x-axis. Bottom Right: silica sphere is now displaced along the y-axis. Bottom Left: silica sphere is now displaced by $0.707\mu m$ along the x and y axis. The trapping beam is a TEM_{00} Gaussian, polarised along the along the x-axis. S_x, S_y, and S_z are shown to the right of each graph, Q_1, Q_2, Q_3, and Q_4 are shown above each graph.

While translational motion have no knock on effects to the QPD signal, rotational changes are between the incident and total fields. This results in rotational motion being biased in the QPD signal - even when collecting signals from isotropic scatterers. To remedy this an inverse rotation is applied to the total field.

To confirm that our method is producing accurate results, we ran a comparison between our simulative QPD and the results from [31]. Where a 300 nm diameter sphere is scanned across the path of a focused Gaussian beam ($\lambda = 1064\ nm$, $NA = 1.2$), the sphere has a refractive index of 1.57 and is suspended in water ($n_{med} = 1.33$) and the condenser lens has its numerical aperture set to 0.5 ($\theta_{max} = 30°$). Scanning across all three primary axis produced the following response curve:

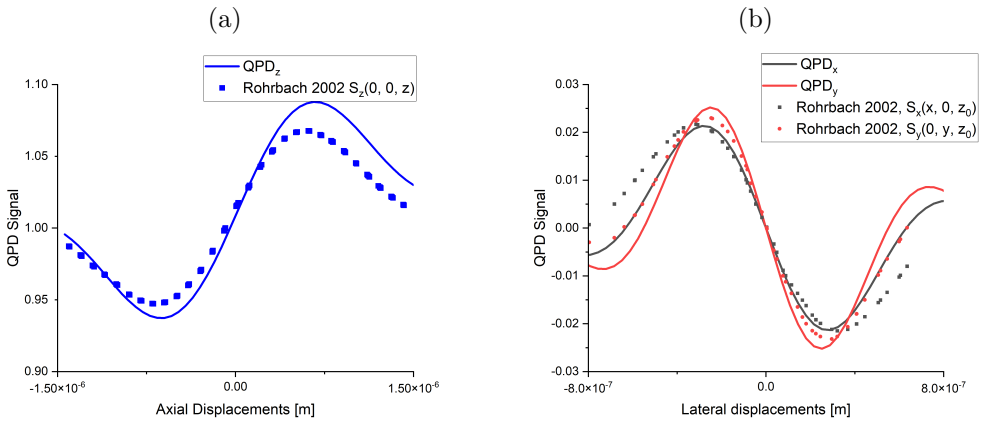

Figure 2.7: Comparison between QPD response signal versus work conducted by Rohrbach, single sphere ($r = 150\ nm$, $n = 1.57$) is scanned by a 1064 nm laser and the QPD signal recorded. Solid lines represent the signal produced by QPD using *ott* and points represent the signal response collected from [31].

The discrepancy between our simulated QPD and the results from Rohrbach can be attributed to the fact that the position to signal error grows as you move further from trap focus. In most optical trapping experiments we usually are calibrating a strong trap where the mean square displacement falls well within the linear regime shown in fig. 2.7. In which case the error between Rohrbach's model and our own is inconsequential for calibration purposes. With this any trajectory can be collected from the QPD by displacing and rotating the beam accordingly, later in chapters **??** and **??** we discuss the limits of accuracy that can be achieved using back focal plane

interferometry to characterise non-spherical targets.

Bibliography

[1] J. D. Jackson, *Classical Electrodynamics*. New York: Wiley, 1975.

[2] T. A. Yasuhiro Harada, "Radiation forces on a dielectric sphere in the rayleigh scattering regime," *Optics Communications*, vol. 124, no. 5-6, pp. 529–541, Mar. 1996. DOI: https://doi.org/10.1016/0030-4018(95)00753-9. [Online]. Available: https://www.sciencedirect.com/science/article/pii/0030401895007539.

[3] M. Capitanio, G. Romano, R. Ballerini, *et al.*, "Calibration of optical tweezers with differential interference contrast signals," *Review of Scientific Instruments*, vol. 73, no. 4, pp. 1687–1696, Apr. 2002, ISSN: 1089-7623. DOI: 10.1063/1.1460929.

[4] A. A. Ranha Neves and C. L. Cesar, "Analytical calculation of optical forces on spherical particles in optical tweezers: Tutorial," *Journal of the Optical Society of America B*, vol. 36, no. 6, p. 1525, Mar. 2019, ISSN: 1520-8540. DOI: 10.1364/josab.36.001525.

[5] Ø. Farsund and B. U. Felderhof, "Force, torque, and absorbed energy for a body of arbitrary shape and constitution in an electromagnetic radiation field," *Physica A*, vol. 227, no. 1–2, pp. 108–130, May 1996, ISSN: 0378-4371. DOI: 10.1016/0378-4371(96)00009-x.

[6] J. H. Crichton and P. L. Marston, "The measurable distinction between the spin and orbital angular momenta of electromagnetic radiation," 2000. [Online]. Available: https://api.semanticscholar.org/CorpusID:16957430.

[7] J. P. Gordon, "Radiation forces and momenta in dielectric media," *Physical Review A*, vol. 8, no. 1, pp. 14–21, Jul. 1973, ISSN: 0556-2791. DOI: 10.1103/physreva.8.14.

[8] W. Li, H. Hu, H. Su, *et al.*, "Numerical analysis on the optical force calculation in the rayleigh scattering regime," *Optical Review*, vol. 28, no. 1, pp. 1–7, Jan. 2021, ISSN: 1349-9432. DOI: 10.1007/s10043-020-00631-7.

[9] P. C. Waterman, "New formulation of acoustic scattering," *The Journal of the Acoustical Society of America*, vol. 45, no. 6, pp. 1417–1429, Jun. 1969, ISSN: 1520-8524. DOI: 10.1121/1.1911619.

[10] T. Wriedt and U. Comberg, "Comparison of computational scattering methods," *Journal of Quantitative Spectroscopy and Radiative Transfer*, vol. 60, no. 3, pp. 411–423, Sep. 1998, ISSN: 0022-4073. DOI: 10.1016/s0022-4073(98)00016-8.

[11] D. W. Mackowski and M. I. Mishchenko, "A multiple sphere t-matrix fortran code for use on parallel computer clusters," vol. 112, pp. 2182–2192, 2011, ISSN: 0022-4073. DOI: 10.1016/j.jqsrt.2011.02.019.

[12] D. W. Mackowski and M. I. Mishchenko, "Calculation of the t matrix and the scattering matrix for ensembles of spheres," *Journal of the Optical Society of America A*, vol. 13, no. 11, p. 2266, Nov. 1996, ISSN: 1520-8532. DOI: 10.1364/josaa.13.002266.

[13] Y.-l. Xu, "Electromagnetic scattering by an aggregate of spheres," *Applied Optics*, vol. 34, no. 21, p. 4573, Jul. 1995, ISSN: 1539-4522. DOI: 10.1364/ao.34.004573.

[14] E. M. Purcell and C. R. Pennypacker, "Scattering and absorption of light by nonspherical dielectric grains," *The Astrophysical Journal*, vol. 186, p. 705, Dec. 1973, ISSN: 1538-4357. DOI: 10.1086/152538.

[15] G. H. Goedecke and S. G. O'Brien, "Scattering by irregular inhomogeneous particles via the digitized green's function algorithm," *Applied Optics*, vol. 27, no. 12, p. 2431, Jun. 1988, ISSN: 1539-4522. DOI: 10.1364/ao.27.002431.

[16] D. T. Gillespie and E. Seitaridou, "The fickian theory of diffusion," in *Simple Brownian Diffusion*. Oxford University Press, Oct. 2012, pp. 1–17. DOI: 10.1093/acprof:oso/9780199664504.003.0001.

[17] D. T. Gillespie and E. Seitaridou, "Einstein's theory of diffusion," in *Simple Brownian Diffusion*. Oxford University Press, Oct. 2012, pp. 38–53. DOI: 10.1093/acprof:oso/9780199664504.003.0003.

[18] D. T. Gillespie and E. Seitaridou, "Implications and limitations of the einstein theory of diffusion," in *Simple Brownian Diffusion*. Oxford University Press, Oct. 2012, pp. 57–73. DOI: 10.1093/acprof:oso/9780199664504.003.0004.

[19] D. T. Gillespie and E. Seitaridou, "Langevin's theory of diffusion," in *Simple Brownian Diffusion*. Oxford University Press, Oct. 2012, pp. 174–190. DOI: 10.1093/acprof:oso/9780199664504.003.0008.

[20] G. Volpe and G. Volpe, "Simulation of a brownian particle in an optical trap," *American Journal of Physics*, vol. 81, no. 3, pp. 224–230, Feb. 2013, ISSN: 1943-2909. DOI: 10.1119/1.4772632.

[21] K. Berg-Sørensen and H. Flyvbjerg, "Power spectrum analysis for optical tweezers," vol. 75, pp. 594–612, 2004, ISSN: 0034-6748. DOI: 10.1063/1.1645654.

[22] S. B. Smith, Y. Cui, and C. Bustamante, "[7] optical-trap force transducer that operates by direct measurement of light momentum," in *Biophotonics, Part B*. Elsevier, 2003, pp. 134–162. DOI: 10.1016/s0076-6879(03)61009-8.

[23] W. Vigilante, O. Lopez, and J. Fung, "Brownian dynamics simulations of sphere clusters in optical tweezers," *Optics Express*, vol. 28, no. 24, p. 36 131, Nov. 2020, ISSN: 1094-4087. DOI: 10.1364/oe.409078.

[24] K. B. Oldham, J. C. Myland, and J. Spanier, "Dawson's integral daw(x)," in *An Atlas of Functions*. Springer US, 2008, pp. 427–433, ISBN: 9780387488073. DOI: 10.1007/978-0-387-48807-3_43.

[25] J. Bang, T. Seberson, P. Ju, *et al.*, "Five-dimensional cooling and nonlinear dynamics of an optically levitated nanodumbbell," *Physical Review Research*, vol. 2, no. 4, p. 043 054, Oct. 2020, ISSN: 2643-1564. DOI: 10.1103/physrevresearch.2.043054.

[26] Yogesha, S. Bhattacharya, and S. Ananthamurthy, "Characterizing the rotation of non symmetric objects in an optical tweezer," *Optics Communications*, vol. 285, no. 10–11, pp. 2530–2535, May 2012, ISSN: 0030-4018. DOI: 10.1016/j.optcom.2012.01.055.

[27] M. Li and J. Arlt, "Trapping multiple particles in single optical tweezers," vol. 281, pp. 135–140, 2008, ISSN: 0030-4018. DOI: 10.1016/j.optcom.2007.09.032.

[28] Yogesha, S. Bhattacharya, and S. Ananthamurthy, "Precise characterization of micro rotors in optical tweezers," *arXiv: Soft Condensed Matter*, 2011. [Online]. Available: https://api.semanticscholar.org/CorpusID:118262469.

[29] T. A. Nieminen, V. L. Y. Loke, A. B. Stilgoe, *et al.*, "Optical tweezers computational toolbox," vol. 9, S196–S203, 2007, ISSN: 1464-4258. DOI: 10.1088/1464-4258/9/8/s12.

[30] A. Nir and A. Acrivos, "On the creeping motion of two arbitrary-sized touching spheres in a linear shear field," *Journal of Fluid Mechanics*, vol. 59, no. 2, pp. 209–223, Jun. 1973, ISSN: 1469-7645. DOI: 10.1017/s0022112073001527. [Online]. Available: http://dx.doi.org/10.1017/S0022112073001527.

[31] A. Rohrbach and E. H. K. Stelzer, "Three-dimensional position detection of optically trapped dielectric particles," *Journal of Applied Physics*, vol. 91, no. 8, pp. 5474–5488, Apr. 2002, ISSN: 1089-7550. DOI: 10.1063/1.1459748.

[32] L. Friedrich and A. Rohrbach, "Tuning the detection sensitivity: A model for axial backfocal plane interferometric tracking," *Opt. Lett.*, vol. 37, no. 11, pp. 2109–2111, Jun. 2012. DOI: 10.1364/OL.37.002109. [Online]. Available: https://opg.optica.org/ol/abstract.cfm?URI=ol-37-11-2109.